What do elliptic flow measurements tell us about the matter created in the little Bang at RHIC?

Roy A. Lacey[*] **and Arkadij Taranenko**

Dept. of Chemistry, Stony Brook University, Stony Brook, NY, 11794-3400, USA.
E-mail: Roy.Lacey@Stonybrook.edu

Elliptic flow measurements are presented and discussed with emphasis on the hydrodynamic character of the hot and dense QCD matter created in heavy ion collisions at RHIC. Predictions from perfect fluid hydrodynamics for the scaling of the elliptic flow coefficient v_2 with eccentricity, system size and transverse energy are validated. A universal scaling for the flow of both mesons and baryons is observed for a broad transverse kinetic energy range when quark number scaling is employed. This suggests a new state of nuclear matter at extremely high density and temperature whose primary constituents have the quantum numbers of quarks and anti-quarks in chemical equilibrium. The scaled flow is used to constrain estimates for several transport coefficients including the sound speed c_s, shear viscosity to entropy ratio η/s, diffusion coefficient (D_c) and sound attenuation length (Γ). The estimated value $\eta/s \sim 0.1$, is close to the absolute lower bound ($1/4\pi$), and may signal thermodynamic trajectories for the decaying matter which lie close to the QCD critical end point.

---

[*]Speaker.

1. Introduction

Recent experiments at Brookhaven's Relativistic Heavy Ion Collider (RHIC), give strong evidence for the creation of locally thermalized hot and dense QCD matter in a "little bang" initiated in ultra relativistic nucleus nucleus collisions [1]. The energy density ε, achieved a short time after the little bang ($\sim 1 fm/c$) has been estimated to be ≥ 5.4 GeV/fm^3 [1] – a value significantly larger than the ~ 1 GeV/fm^3 required for the transition from hadronic matter to the high-temperature plasma phase of QCD [2, 3]. A confluence of experimental results [1, 4, 5, 6] now suggest that this new state of matter bears strong kinship to the hot and dense plasma of quarks and gluons (QGP) produced a few micro seconds after the "big bang" that gave birth to our universe some $12 - 14$ billion years ago. Now, the scientific challenge is to explore robust experimental constraints which can establish the detailed properties of this QGP.

In this contribution, we show experimental validation for; (i) the scaling predictions of perfect fluid hydrodynamics for the elliptic flow coefficient v_2, (ii) the development of elliptic flow in the pre-hadronization phase, (iii) the scaling of D meson flow compatible with full thermalization of the charm quark and (iv) universal scaling of the flow of both mesons and baryons (over a broad transverse kinetic energy range) via quark number scaling. Subsequently, we use the scaled flow values to constrain a number of transport coefficients.

2. Thermalization and harmonic flow correlations

Local thermalization plays a central role in considerations involving perfect fluid hydrodynamics. Consequently, it is important to recap a few of the key observables which are consistent with the production of high energy density thermalized matter at RHIC [7]. In brief;

- the multiplicity distribution for the same number of participants is independent of colliding system size as would be expected from a system which "forgets" how it is formed. A demonstration of this independence hypothesis has been given for Au+Au and Cu+Cu collisions by the PHOBOS collaboration [8].

- A comparison of the measured anti-particle to particle yield ratios $\bar{p}/p$, to the predictions of a statistical model

$$\frac{\bar{p}}{p} = \frac{e^{-(E+\mu)/T}}{e^{-(E-\mu)/T}} = e^{-2\mu/T},$$
(2.1)

show excellent agreement for a single temperature T and baryon chemical potential μ [9].

- Surprisingly large harmonic flow correlations compatible with the development of sizable pressure gradients in a locally thermalized fluid are observed for a broad selection of hadrons comprised of light- and heavy quark combinations ($\pi, K, p, \Lambda, \Omega, \phi, \Xi, d, D, \ldots$) [10, 11, 12, 13, 14]. We emphasize here that rather strong interactions are required in this fluid to generate significant flow for hadrons comprised of a heavy quark, ie. the heavy quark relaxation time is much longer than that for the light quarks.

The magnitude of harmonic flow correlations is commonly characterized by the Fourier coefficients v_n as [15]:

$$v_n \equiv \langle e^{in(\varphi - \Phi_R)} \rangle = \langle \cos n(\varphi - \Phi_R) \rangle,$$
(2.2)

where φ is the azimuthal angle of an emitted particle (measured in the laboratory coordinate system) and Φ_R is an estimate of the azimuth of the reaction plane. A correction factor for v_n is usually required to take account of the dispersion of the estimated reaction plane [16, 17, 18]. The second harmonic coefficient v_2 is termed elliptic flow.

At RHIC energies, it is widely believed that elliptic flow results from hydrodynamic pressure gradients developed in an initial "almond-shaped" collision zone. That is, the initial transverse coordinate-space anisotropy of the collision zone is converted, via particle interactions, into an azimuthal momentum-space anisotropy. Elliptic flow self-quenches due to expansion of the collision zone. Consequently, rapid local thermalization is required to achieve relatively large v_2 signals. The current consensus is that the sizable values observed at RHIC are compatible with the hydrodynamic expansion of a near perfect fluid.

3. Universal scaling and perfect fluid hydrodynamics

Perfect fluid hydrodynamics stipulates that the constituents of a fluid flow with the same velocity field. In many hydrodynamic models [19, 20, 21, 22, 23, 24, 25], elliptic flow results from pressure gradients due to the initial spatial asymmetry or eccentricity $\varepsilon = (\langle y^2 - x^2 \rangle)/(\langle y^2 + x^2 \rangle)$, of the high energy density matter in the collision zone. The initial entropy density $S(x,y)$, is often used to perform an average over the x and y coordinates of the matter in the plane perpendicular to the collision axis. For a system of transverse size $\bar{R}$ $(1/\bar{R} = \sqrt{1/\langle x^2 \rangle + 1/\langle y^2 \rangle})$, this flow develops over a time scale $\sim \bar{R}/\langle c_s \rangle$ for matter with sound speed c_s [25]. Thus, the initial energy density controls how much flow develops globally, while the detailed development of the flow correlation patterns are governed by ε and c_s. Centrality dependent differential measurements give clear access to ε; access to c_s is less direct but is reflected in the magnitude of the flow. Lattice QCD calculations indicate that $c_s^2 \approx 1/3$ for $T > 2T_c$, but drops steeply by more than a factor of six near the "softest point" where $T \approx T_c$ ie. the critical temperature [26]. Thereafter, it rises again in the hadron resonance gas phase to the value $c_s^2 \approx 0.15$ for SPS energies.

A remarkable empirical fact recently reported, is the observation that universal scaling for the flow of both mesons and baryons is achieved when $v_2/n_q \varepsilon$ is plotted vs. KE_T/n_q [28, 29]. Here, n_q is the number of valence quarks ($n_q = 2, 3$ for mesons and baryons respectively) and $KE_T = m_t - m$ is the transverse kinetic energy[1]. Further demonstration of this scaling is illustrated via Figs. 1 and 2. Figure 1 shows differential flow measurements $v_2(p_T)$, for several particle species produced at mid-rapidity in central and semi-central Au+Au collisions at $\sqrt{s_{NN}} = 200$ GeV; they span essentially the full range of measurements (several hundred data points) at RHIC. The v_2 values shown for charged and neutral pions ($\pi^\pm$, π^0), charged kaons ($K^\pm$), (anti-) protons (($\overline{p}$)p), (anti-) deuterons (($\overline{d}$)d) and the ϕ meson represent recent measurements (published and preliminary results) obtained by the PHENIX collaboration [7, 27, 28, 29]. The values for neutral kaons (K_S^0), lambdas ($\Lambda + \bar{\Lambda}$), cascades ($\Xi + \bar{\Xi}$) and omegas ($\Omega + \bar{\Omega}$) show results from the STAR collaboration [11, 13, 31, 30].

The most striking feature of this plot is the large magnitude of $v_2(p_T)$ observed for all particle species. Fig. 2 shows the scaled results obtained from the same data. It indicates that the relatively

---

[1]The pressure in an ideal gas can be seen to be a measure of its kinetic energy density.

complicated "fine structure" of v_2 (ie. its detailed dependence on centrality, transverse momentum, particle type, etc) for particles produced at mid-rapidity can be scaled to a single function.
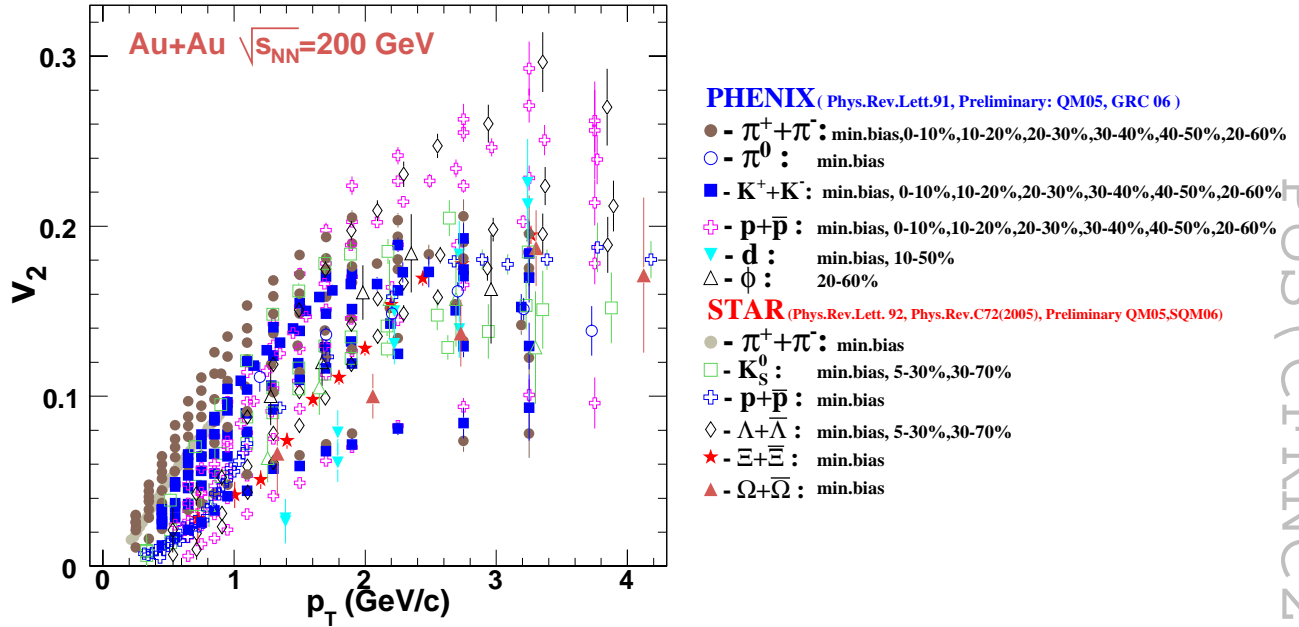

Figure 1: v_2 vs. p_T for several particle species produced at midrapidity in central and semi-central Au+Au collisions at $\sqrt{s_{NN}} = 200$ GeV. The centrality and particle species selections are indicated.
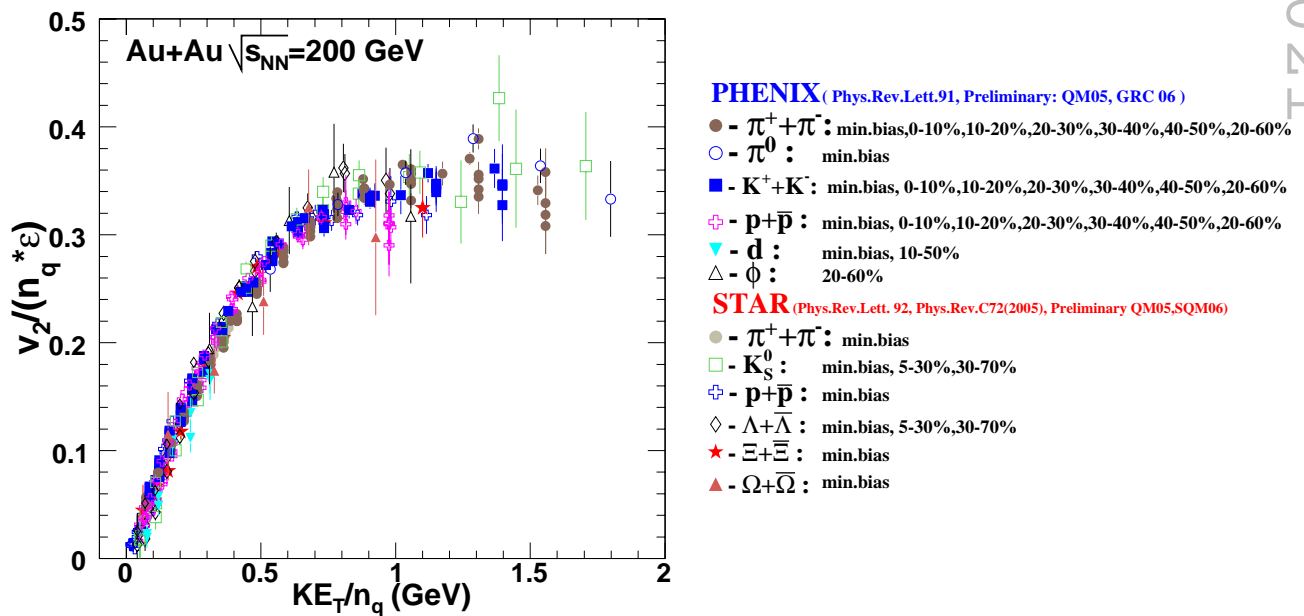

Figure 2: $v_2/n_q\varepsilon$ vs. KE_T/n_q for several particle species produced at midrapidity in central and semi-central Au+Au collisions at $\sqrt{s_{NN}} = 200$ GeV. The data selections are indicated.
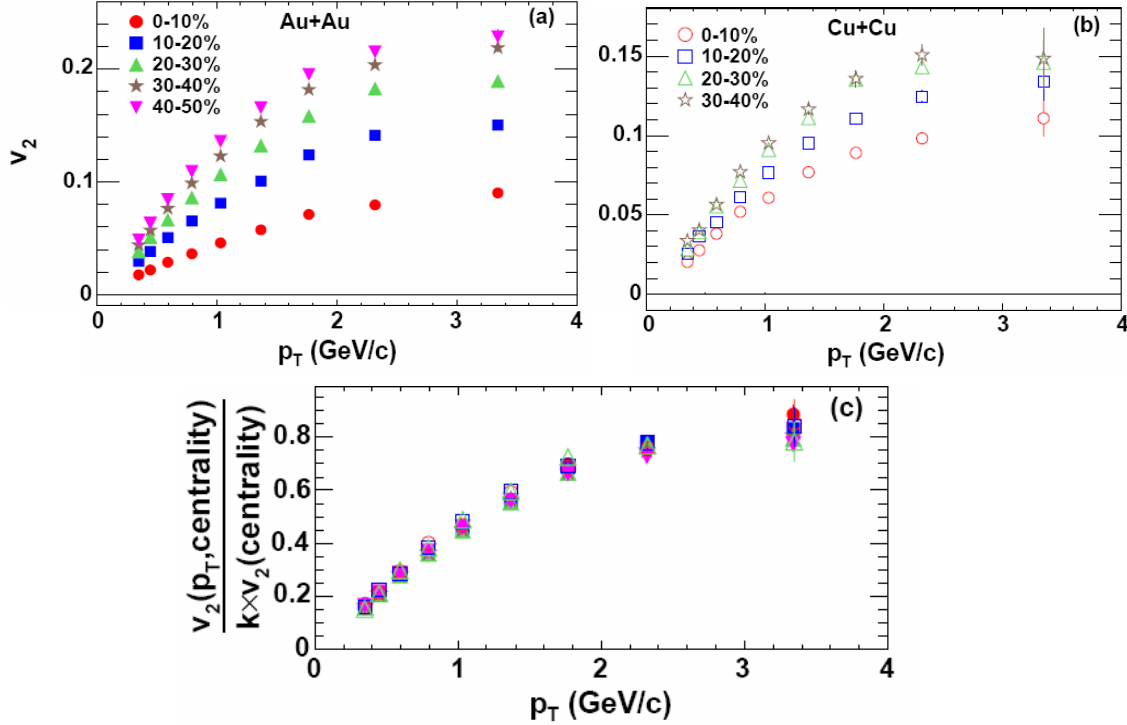
Figure 3: v_2 vs. p_T for charged hadrons obtained in Au+Au (a) and Cu+Cu (b) collisions for several centralities as indicated. Panel (c) shows $v_2(centrality, p_T)$ divided by k times the p_T-integrated value $v_2(centrality)$, for Au+Au and Cu+Cu ($k = 3.1$ see text and Refs. [28, 29]).

On the one hand, this universal scaling validates the predictions of perfect fluid hydrodynamics [20, 25, 32, 33, 34]. That is;

- $v_2(p_T)/\varepsilon$ should be independent of centrality;

- $v_2(p_T)$ should be independent of colliding system size for a given eccentricity;

- for different particle species, $v_2(KE_T)$ at mid-rapidity should scale with the transverse kinetic energy $KE_T = m_T - m$, where m_T is the transverse mass of the particle;

- $v_4(p_T) \propto v_2^2(p_T)$.

On the other hand, it corroborates the n_q scaling expected from quark coalescence models [35, 36, 37, 38] suggesting that quark-related degrees of freedom are present when elliptic flow develops.

These separate aspects of the observed universal scaling are illustrated in Figs.3 and 4. Figures 3a and 3b show the differential $v_2(p_T)$ for charged hadrons obtained in Au+Au and Cu+Cu collisions respectively. The expected increase in $v_2(p_T)$ as collisions become more peripheral and the p_T increases [1, 4, 5] is unmistakable. Fig. 3c show the resulting ε-scaled values for both systems. The eccentricity is obtained from the p_T-integrated v_2 values i.e. $\varepsilon = k \times v_2$. A Glauber model estimate of ε in Au+Au collisions [39] gives $k = 3.1 \pm 0.2$ for the cuts employed in the analysis [28, 29].
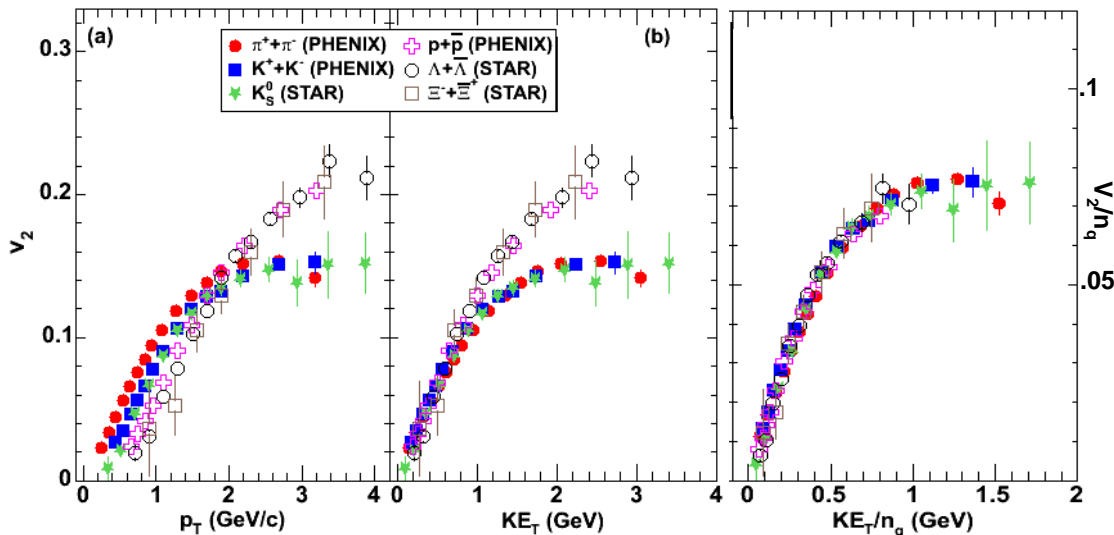
Figure 4: v_2 vs. p_T (left panel) and KE_T (middle panel). The scaled results in the right panel is obtained by n_q scaling the data shown in the middle panel. Results are shown for several particle species produced in minimum bias Au+Au collisions at $\sqrt{s_{NN}} = 200$ GeV [29].

These scaled values shown in Fig. 3c validate the expected independence on colliding system size [7, 25] and suggests that rapid local thermalization [40, 41] is achieved. They also allow an estimate of c_s because the magnitude of v_2/ε depends on the sound speed c_s [25]. A recent estimate [28, 29] gives $c_s \sim 0.35 \pm 0.05$; a value which suggests an effective equation of state (EOS) which is softer than that for the high temperature QGP [26]. It however, does not reflect a strong first order phase transition in which $c_s = 0$ during an extended hadronization period. Such an EOS could very well be the reason why $v_2(p_T)$ is observed to saturate in Au+Au collisions for the collision energy range $\sqrt{s_{NN}} = 60 - 200$ GeV [42].

The other aspects[2] of the observed universal scaling are illustrated in Fig.4. The left panel show measurements of the p_T dependence of v_2 for several particle species. The middle panel bears out the expected particle mass scaling when v_2 is plotted vs. KE_T. For $KE_T \geq 1$ GeV, clear splitting into a meson branch (lower v_2) and a baryon branch (higher v_2) occurs. However, both of these branches show rather good scaling separately. The right panel shows the resulting values obtained after scaling both v_2 and KE_T (ie the data in the middle panel) by n_q. This latter scaling is an indication of the inherent quark-like degrees of freedom in the flowing matter. That is, we assert that the bulk of the elliptic flow develops in the pre-hadronization phase.

3.0.1 Validation of the pre-hadronic development of elliptic flow

Despite robust quark number scaling, one can still ask whether or not the bulk of the elliptic flow develops pre- or post-hadronization. This question can be readily addressed via careful study of the v_2 for the ϕ meson. The ϕ meson is comprised of a strange (s) and an anti-strange ($\bar{s}$) quark

---

[2]Validation of the hydrodynamic scaling prediction that $v_4 \propto v_2^2$ is presented in Ref. [7]. It is a non-trivial prediction; the measured differential $v_2(p_T)$ show a linear p_T dependence for low p_T pions but $v_4(p_T)$ is quadratic in p_T.
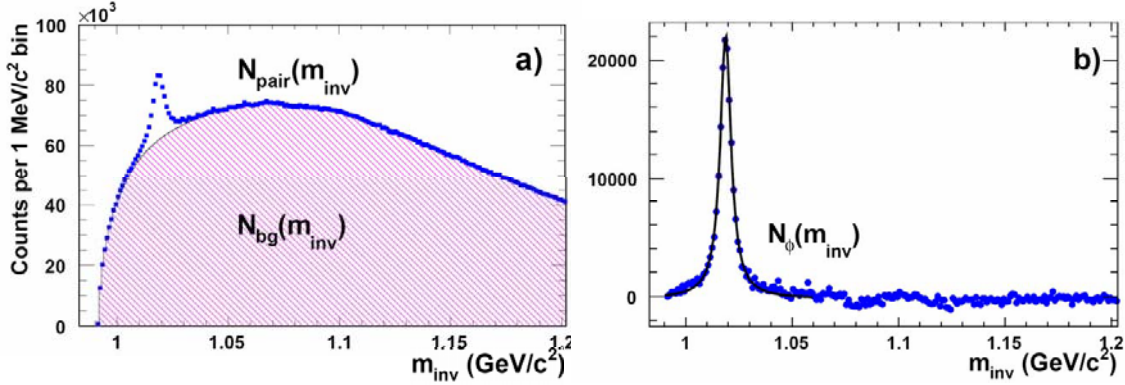
Figure 5: (Color on line) An example of invariant mass distributions for K^+K^- pairs identified in the PHENIX detector for p_T^{pair}=1.6-2.7 GeV/c and reaction centrality 20-60%: The left panel shows the distribution for signal plus combinatoric background. The right panel shows the distribution after background subtraction.

and its interaction with nuclear matter is suppressed according to the Okubo-Zweig-Izuka (OZI) rules [43]. Therefore, the ϕ meson is expected to have a rather small hadronic cross section with non-strange hadrons ($\sim$ 9 mb) [44, 45, 46] and this leads to the relatively large mean free path λ_ϕ, when compared to the transverse size of the emitting system.

Thus, if elliptic flow was established in a phase involving hadrons interacting with their standard hadronic cross sections (post-hadronization), one would expect v_2 for the ϕ to be significantly smaller than that for other hadrons (eg. p and π). An added bonus is that the relatively long lifetime ($\sim$ 45 fm/c) for the ϕ makes its decay inside the pre-hadronization medium unlikely and this makes for a cleaner measurement. For these reasons, flow measurements for the ϕ play a crucial role for the distinction between pre- and post-hadronic development of elliptic flow [47].

The elliptic flow measurements for the ϕ meson are made difficult due to combinatoric background; for the case presented here, such a background results from K^+K^- pairs which do not come from the decay of the ϕ. Figures 5**a** and **b** show a typical example of invariant mass distributions for K^+K^- pairs obtained in Au+Au collisions at $\sqrt{s_{NN}} = 200$ GeV. These preliminary data show results before and after combinatorial background subtraction. Here, it is important to stress that the combinatorial background also exhibits an azimuthal anisotropy (v_2) which needs to be separated from that for the ϕ meson. This can be achieved via a technique recently developed by Borghini et al. [48]. The technique which is based on the study of v_2 as a function of invariant mass, allows for robust v_2 extraction even for a rather small signal-to-background ratio. Needless to say, the distributions shown in Fig 5 allow a very reliable v_2 measurement for the ϕ meson.

The left and right panels of Fig. 6 compares the unscaled and scaled results (respectively) for v_2 vs. KE_T for π, K, p and ϕ in 20-60% central Au+Au collisions at $\sqrt{s_{NN}} = 200$ GeV. These are recent preliminary results obtained by the PHENIX collaboration. The left panel clearly shows that, despite its mass which is comparable to that for the proton, $v_2(KE_T)$ for the ϕ follows the flow pattern of the other light mesons (π and K) whose cross sections are not OZI suppressed. The right panel indicate the expected universal scaling after n_q scaling. We therefore conclude that, when elliptic flow develops, the constituents of the flowing medium can not be ground state hadrons
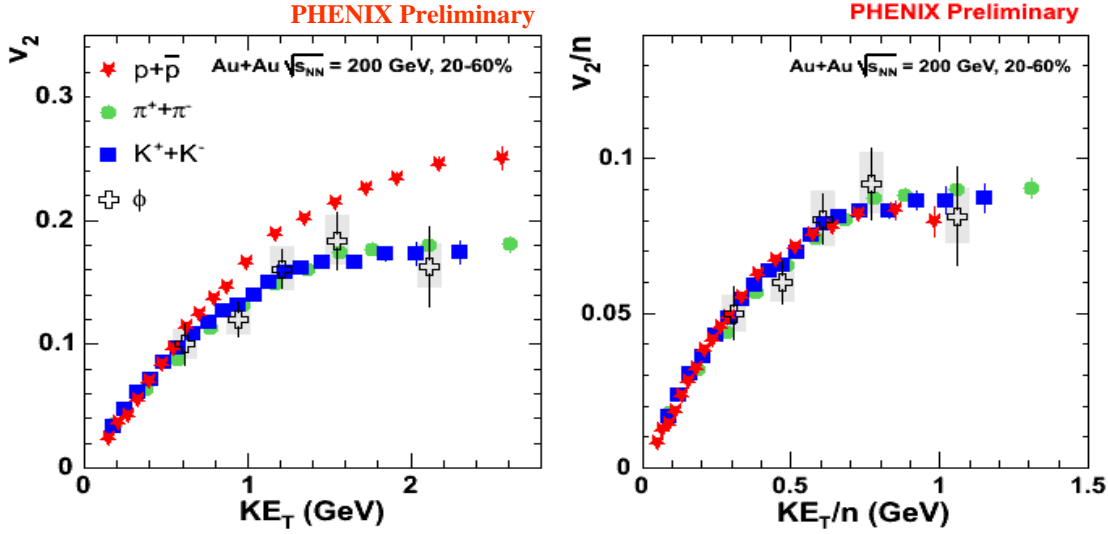
Figure 6: (Color on line) Comparison of v_2 vs. KE_T for π, K, p and ϕ mesons (left panel) detected in semi-central (20-60%) Au+Au collisions at $\sqrt{s_{NN}} = 200$ GeV. The right panel show the same data scaled by quark number. These preliminary data have been obtained by the PHENIX collaboration.

interacting with their standard hadronic cross sections. Instead, they reflect a pre-hardonization state of the created high energy density matter that contain the prerequisite quantum numbers of the hadrons to be formed ie. the QGP. It is noteworthy that a similar investigation can be made via v_2 measurements for "heavy" multi-strange baryons such as the $\Omega + \bar{\Omega}$; they too, are expected to have a relatively small hadronic scattering cross section. Indeed, we have observed that the recent high-statistics preliminary STAR results for $\Omega + \bar{\Omega}$ v_2 in Au+Au collisions at $\sqrt{s_{NN}} = 200$ GeV (presented at SQM 2006) [31, 30] do follow the universal v_2/n_q vs KE_T/n_q scaling (see Fig 2).

3.1 Validation of charm quark diffusion and flow

As indicated earlier, perfect fluid hydrodynamics stipulates that all constituents of the QGP should experience the same velocity field. This requirement places severe constraints on the flow of heavy quarks and their attendant hadrons because their relaxation time τ_R is much larger than that for light quarks [49];

$$\tau_R \sim \frac{M}{T} \Gamma_s,$$

where M is the mass of the heavy quark, T is the temperature and $\Gamma_s = \eta/sT$ is an estimate of the light quark relaxation time; η and s are the viscosity and entropy density respectively. For the charm quark ($M \sim 1.4$ GeV) at a temperature of 165 MeV, this translates into an ~ 8 fold increase compared to Γ_s. Heavy quarks are also produced with a power-law or non-thermal transverse momentum spectrum. Thus, one might expect the elliptic flow for heavy quarks to be much smaller than that for light quarks (for reasonable system lifetimes), unless in-medium interactions are strong enough to enforce many interactions with sufficient momentum transfer to thermalize them.
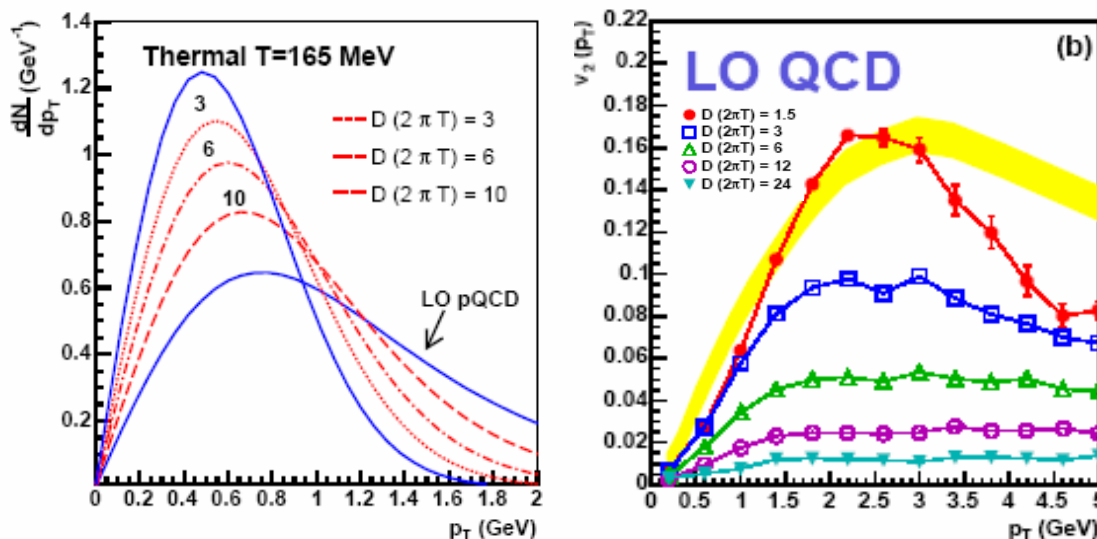
Figure 7: (Color on line) (a) Evolution of charm quark transverse momentum spectrum with different values of the diffusion coefficient D_c as indicated. The thermal spectrum for $T = 165$ MeV and the initial transverse momentum spectrum given by leading order perturbation theory (LO pQCD) are indicated. (b) Evolution of charm quark $v_2(p_T)$ with D_c. These figures are taken from Ref. [49].

The heavy quark diffusion coefficient D_{hq}, is related to τ_R [49];

$$\tau_R = \frac{M}{T} D_{hq}$$

Thus, D_{hq} ultimately controls the extent to which the initial power-law spectrum approaches the thermal spectrum and the extent to which the heavy quark will follow the underlying flow of the medium. This is illustrated for the charm quark in Fig. 7 [49] where the evolution of the p_T distribution and the differential $v_2(p_T)$, are shown for different values of the charm quark diffusion coefficient D_c. The figure clearly indicates that measurements of charm quark differential elliptic flow $v_2(p_T)$ can serve to constrain D_c.

One method of accessing charm v_2 is to measure the the elliptic flow of "non-photonic" electrons that originate primarily from the semi-leptonic decays of D and B mesons. Such a measurement has been made recently and found to yield significant anisotropy for D mesons [14].

Figures 8a and b show differential $v_2(p_T)$ results obtained for non-photonic electrons and D mesons respectively. The D meson results reflect estimates for $p_T < 2.0$ GeV/c, obtained via detailed simulations constrained by the differential measurement $v_2(p_T)$ for non-photonic electrons [14]. For these simulations, the p_T spectrum was constrained by data and all non-photonic electrons were assumed to come from D meson decay [14]. Estimates were obtained for three separate **shape** assumptions for $v_2(p_T)$ for the D mesons. The result from each is show in 8b.

These results indicate clear evidence that the D meson and consequently the charm quark, do flow with a large v_2. This suggest that the in-medium interactions are strong and perhaps frequent enough to thermalize the charm quark. If this is indeed the case, then $v_2(KE_T)$ for the D meson should show the same universal scaling presented earlier for other hadrons.
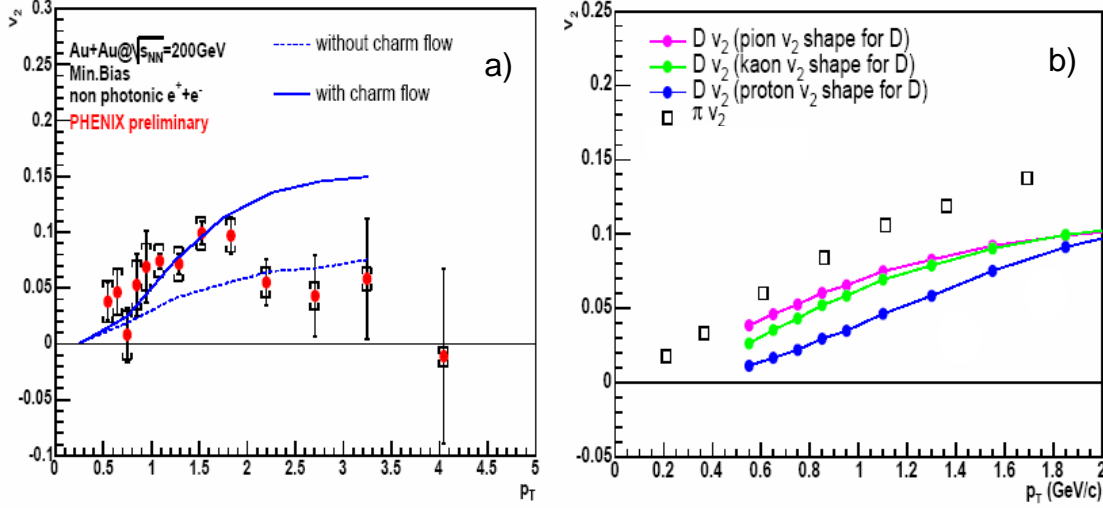
Figure 8: (Color on line) (a) v_2 vs. p_T for non-photonic electrons. The solid and dashed lines compare the results from a calculation which includes/excludes charm flow [50]. (b) v_2 vs. p_T for D mesons derived from the non-photonic electron measurements for $p_T < 2.0$ GeV/c. Results are shown for several assumptions for the shape of the p_T dependence of the D meson v_2. The results for pions are shown for comparison.

Figures 9a and b compare the unscaled and scaled results (respectively) for v_2 vs. KE_T for π, K, p and D mesons measured in minimum bias Au+Au collisions. The assumed shape for the transverse momentum dependence of the D meson v_2 is that for the proton cf. Fig. 8b. We note here that this assumption is compatible with a large array of differential flow measurements for different "heavy" particle species (see for example Refs. [11, 13, 31, 30]). Both panels (a and b) of Fig. 9 show robust scaling; they confirm that the D mesons (for $p_T < 2.0$ GeV/c) and their associated charm quarks flow with a fluid velocity field identical to that of the other constituents. This means that the medium responds as a thermalized fluid and the transport mean free path is small.

The filled triangles in Fig. 9 show results from an approximate interpolation of the model estimates for the charm quark [49] presented in Fig. 7b. In Fig. 9 these estimates are shown only for $p_T \leq 2.0$ GeV/c ie. the available range of the D meson data[3]; they are close to the ones obtained from the LO-QCD charm quark spectrum for a calculation in which $D_c \sim 3/2\pi T$ (see. Fig. 7b). We note here that the calculations are for the charm quark and do not include the effects of hadronization/fragmentation leading to D meson production. Despite the many caveats of the model [49], Fig. 9 shows that v_2 for the charm quark can be made to follow universal scaling for an appropriate choice of the coefficient D_c. It is noteworthy that an even smaller value $D_c \sim 1.5/2\pi T$ is found if the drag on the charm quark is made to depend on the velocity ie. $dp/dt \propto v$.

4. Transport properties of the high energy density fluid

The observed scaling of elliptic flow provide important constraints for the transport properties

---

[3]The indicated scaling is observed to break for charm quarks with $p_T > 2.0$ GeV/c. Thus, high p_T measurements are critical to the development of further constraints.
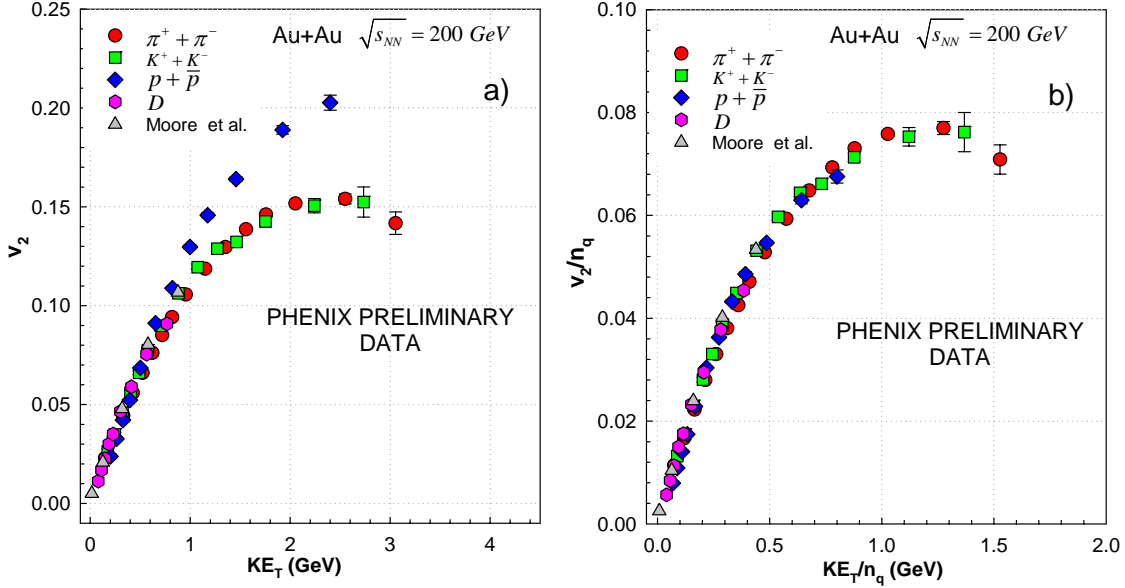
Figure 9: (Color on line) (a) v_2 vs. KE_T. (b) v_2/n_q vs. KE_T/n_q. Results are shown for several particle species produced in minimum bias Au+Au collisions at $\sqrt{s_{NN}} = 200$ GeV. Interpolated results from a model calculation [49] for charm quarks are also indicated.

of the high energy density QGP fluid. In what follows, we apply several of these constraints to make estimates for a number transport coefficients.

4.1 Time scale for the development of elliptic flow

As discussed earlier, elliptic flow develops gradually in the evolving system on a time scale τ characterized by its transverse size $\bar{R}$ and the sound speed c_s:

$$\tau \sim \frac{\bar{R}}{c_s}. \tag{4.1}$$

Values for $\bar{R}$ have been reported as a function of centrality in Ref. [25] for Au+Au collisions at $\sqrt{s_{NN}} = 60 - 200$ GeV. They indicate little change over the centrality range of interest here, so we use an averaged value $\langle \bar{R} \rangle \sim 1.9$. The value $\langle c_s \rangle = 0.35 \pm 0.05$ determined via eccentricity scaling was presented earlier. These values give $\langle \tau \rangle \sim \langle \bar{R} \rangle / \langle c_s \rangle \sim 5.4$ fm, ie. the mean time required to "translate" the initial spatial anisotropy of the high energy density fluid into a momentum anisotropy.

4.2 The viscosity to entropy ratio η/s

Validation of the predictions from perfect fluid hydrodynamics for the scaling of the elliptic flow demands a low shear viscosity to entropy ratio (η/s) for the high energy density matter created. On the one hand, this is very well supported by the observation that experimental v_2 values are in fairly good agreement with simulated values based upon ideal hydrodynamics [40, 41, 21, 52]. On the hand the predicted suppression of flow, due to shear viscosity, by weak-coupling transport

11

calculations is not observed. However, η/s cannot be arbitrarily small because quantum mechanics limits the size of cross sections via unitarity. An absolute lower bound is $1/4\pi$, reached in the strong coupling limit of certain gauge theories. This bound has been recently conjectured to hold for all substances [53].

The observed universal scaling of v_2 can be used to constrain a reliable estimate for η/s [54, 55]:

$$\frac{\eta}{s} \sim T\lambda_f c_s, \tag{4.2}$$

where T is the temperature, λ_f is the mean free path and c_s is the sound speed in the matter. The temperature $T = 165 \pm 3$ MeV was obtained via a hydrodynamically inspired fit to the scaled data shown in Fig. 2. The functional form used for the fit is $I_1(w)/I_0(w)$, where $w = KE_T/2T$ and $I_1(w)$ and $I_0(w)$ are Bessel functions [34]. For c_s, we use the estimate $c_s = 0.35 \pm 0.05$, given earlier and in Refs. [28] and [29]. The mean free path estimate $\lambda_f = 0.3 \pm 0.03 fm$, was obtained from an on-shell transport model simulation of the gluon evolution (in space and time) in Au+Au collisions at 200 GeV [56]. This parton cascade model includes pQCD $2 \leftrightarrow 2$ and $2 \leftrightarrow 3$ scatterings. These values for λ_f, T and c_s lead to the estimate $\eta/s \sim 0.09 \pm 0.015$ with an estimated systematic error of $+0.1$ primarily due to uncertainties in λ_f.

This estimated value for η/s is in good agreement with the experimentally based estimates of Teaney and Gavin [57, 58] and the theoretical estimates of Gyulassy and Shuryak [52, 59]. However, it is much lower than the value obtained from weak coupling QCD [61] or hadronic computations [60]. This low value for η/s has been interpreted as evidence that the QGP is more strongly coupled than previously thought [40, 52].

4.3 The bulk viscosity

Two component models (see for example Ref. [51]) are often used to estimate the bulk viscosity ς. Assuming such a model holds here, the bulk viscosity can be expressed in terms of the shear viscosity and the sound speed as:

$$\varsigma = \frac{5}{3}\left(1 - 3c_s^2\right)^2. \tag{4.3}$$

Using the value $\langle c_s \rangle = 0.35$, we find the relation $\langle \varsigma \rangle \sim 0.7\eta$. Thus, the implication is that the time averaged bulk viscosity of the high energy density matter is also relatively small but non-zero. Here, it is important to stress that for higher temperatures (eg. $T \sim 2T_c$), lattice QCD calculations give $c_s^2 \sim 1/3$ which leads to $\varsigma \sim 0$. This implies that much of the bulk viscosity develops at the lower temperatures close to T_c.

4.4 The sound attenuation length

With T and η/s in hand, the sound attenuation length Γ_s, can be evaluated as:

$$\Gamma_s = \frac{4}{3}\frac{\eta}{sT}. \tag{4.4}$$

This gives $\Gamma_s \sim 0.16$ fm and $\eta/Ts \sim 0.12$ fm. These values suggests a rather short relaxation time for light quarks.

4.5 The Reynolds R_e and Knudsen K_n numbers

The Reynolds R_e and Knudsen K_n numbers play an important role in hydrodynamic considerations;

$$R_e \equiv \frac{\varepsilon \bar{R} c_s}{\eta}. \tag{4.5}$$

Here ε is the energy density. A large Reynolds number indicates that viscous forces are not important to the flow. That is, the smallest scales of fluid motion are undamped.

The Knudsen number is given as:

$$K_n = \frac{\lambda}{\bar{R}}; \tag{4.6}$$

its reciprocal gives a measure of the number of collisions per particle. Thus, Local thermal equilibrium is expected if $K^{-1} >> 1$.

Since the shear viscosity η can be expressed as:

$$\eta = \varepsilon \lambda c_s, \tag{4.7}$$

and flow is transonic (ie. Mach number $M_n \sim 1$),

$$R_e \sim \frac{1}{K_n}. \tag{4.8}$$

Using the previously obtained values for λ and $\bar{R}$ we obtain $K^{-1} \sim 6$. Such a large number favors rapid local thermalization.

4.6 Diffusion coefficient D_c for the charm quark

The diffusion coefficient D_c, for the charm quark is related to its relaxation time τ_R [49];

$$\tau_R = \frac{M}{T} D_c. \tag{4.9}$$

As discussed earlier, it controls the extent to which the initial power-law spectrum for the charm quark approaches the thermal distribution and the extent to which it follows the underlying flow of the medium.

The agreement between theory and experiment shown in Fig. 9, was achieved for

$$D_c \sim \frac{3}{2\pi T}. \tag{4.10}$$

This gives the values $D_c \sim 0.6$ fm and $\tau_R \sim 5$ fm. Thus, D_c is approximately a factor of five times larger than the hydrodynamic scale η/sT but τ_R is similar to the time for the development of elliptic flow.

4.6.1 Does the value of η/s signal the QCD critical end point?

Our earlier estimate of the viscosity to entropy ratio is indicated by the filled hexagon is shown in Fig. 10. This figure shows η/s vs $(T - T_c)/T_c$ for molecular, atomic and nuclear matter. The data for He, N_2 and H_2O were obtained for their respective critical pressure. They are taken from Ref. [66] and the references therein. The calculated results shown for the meson-gas (for $T < T_c$)
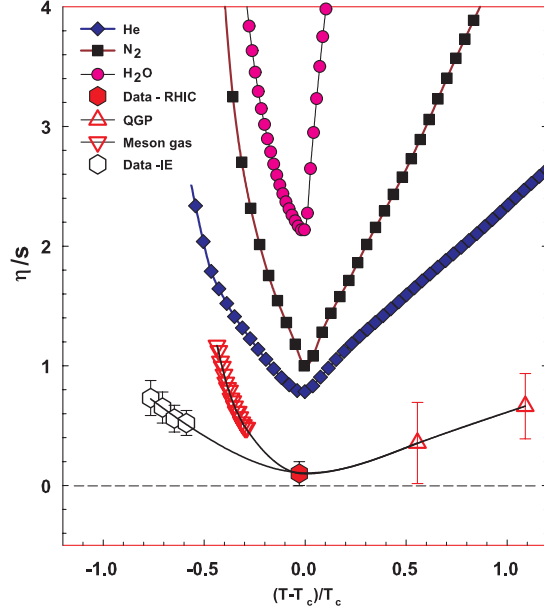
Figure 10: (Color online) η/s vs $(T - T_c)/T_c$ for several substances as indicated. The calculated values for the meson-gas have an associated error of $\sim 50\%$ [62]. The lattice QCD value $T_c = 170$ MeV [63] is assumed for nuclear matter. The lines are drawn to guide the eye.

are obtained from chiral perturbation theory with free cross sections [62]. Those for the QGP (ie. for $T > T_c$) are from lattice QCD simulations [67]. The value $T_c \sim 170$ MeV is taken from lattice QCD calculations [63].

Figure 10 illustrates the observation that for atomic and molecular substances, the ratio η/s exhibits a minimum of comparable depth for isobars passing in the vicinity of the liquid-gas critical point [53, 66]. When an isobar passes through the critical point (as shown in Fig. 10), the minimum forms a cusp at T_c; when it passes below the critical point, the minimum is found at a temperature below T_c (liquid side) but is accompanied by a discontinuous change across the phase transition. For an isobar passing above the critical point, a less pronounced minimum is found at a value slightly above T_c. The value η/s is smallest in the vicinity of T_c because this corresponds to the most difficult condition for the transport of momentum [66].

Given these observations, one expects a broad range of trajectories in the (T, n_B) or (T, μ_B) plane for nuclear matter, to show η/s minima with a possible cusp at the critical point. The exact location of this point is of course not known, and only coarse estimates of where it might lie are available. The open triangles in the figure show calculated values for η/s along the $\mu_B = 0$, $n_B = 0$ trajectory. For $T < T_c$ the η/s values for the meson-gas show an increase for decreasing values of T. For T greater than T_c, the lattice results [67] indicate an increase of η/s with T, albeit with large error bars. These trends suggest a minimum for η/s in the vicinity of T_c. This minimum is rather close to the absolute lower bound of $\eta/s = 1/4\pi$. We therefore speculate that it is compatible with the minimum expected if the hot and dense QCD matter produced in RHIC collisions follow decay trajectories which are close to the QCD critical end point (CEP). Such trajectories could

be readily followed if the CEP acts as an attractor for thermodynamic trajectories of the decaying matter [64, 65].

5. Summary

In summary, elliptic flow measurements at RHIC provide compelling evidence for the production and rapid thermalization (less than 1 fm/c after impact) of a new state of matter having an energy density well in excess of the critical value required for de-confinement i.e the QGP. Validation of the predictions from perfect fluid hydrodynamics for the scaling of the elliptic flow, in conjunction with the universal scaling of baryons and mesons (via quark number), serve as constraints for the extraction of several transport coefficients for this matter. These coefficients give important insights on the transport properties and the decay dynamics of the QGP and suggest a plasma having essentially perfect liquid-like properties.

References

[1]   K. Adcox *et al.* [PHENIX Collaboration], Nucl. Phys. A **757** (2005) 184

[2]   F. Karsch, Nucl. Phys. A **698** (2002) 199

[3]   Z. Fodor and S. D. Katz, JHEP **0203** (2002) 014

[4]   J. Adams *et al.* [STAR Collaboration], Nucl. Phys. A **757** (2005) 102

[5]   B. B. Back *et al.*, [PHOBOS Collaboration], Nucl. Phys. A **757** (2005) 28

[6]   I. Arsene *et al.* [BRAHMS Collaboration], Nucl. Phys. A **757** (2005) 1

[7]   R. A. Lacey, Nucl. Phys. A **774** (2006) 199

[8]   G. Roland *et al.* [PHOBOS Collaboration], Nucl. Phys. A **774** (2006) 113

[9]   P. Braun-Munzinger, D. Magestro, K. Redlich and J. Stachel, Phys. Lett. B **518** (2001) 41

[10]   S. S. Adler *et al.* [PHENIX Collaboration], Phys. Rev. Lett. **91** (2003) 182301

[11]   J. Adams *et al.* [STAR Collaboration], Phys. Rev. Lett. **92** (2004) 052302

[12]   J. Adams *et al.* [STAR Collaboration], Phys. Rev. C **72** (2005) 014904

[13]   J. Adams *et al.* [STAR Collaboration], Phys. Rev. Lett. **95** (2005) 122301

[14]   S. Sakai, [PHENIX Collaboration], nucl-ex/0510027.

[15]   S. Voloshin and Y. Zhang, Z. Phys. C **70** (1996) 665

[16]   P. Danielewicz and G. Odyniec, Phys. Lett. B **157**, 146 (1985).

[17]   A. M. Poskanzer and S. A. Voloshin, Phys. Rev. C **58**, 1671 (1998) [nucl-ex/9805001].

[18]   J.-Y. Ollitrault, nucl-ex/9711003.

[19]   J. Y. Ollitrault, Phys. Rev. D **46** (1992) 229.

[20]   H. Heiselberg and A. M. Levy, Phys. Rev. C **59** (1999) 2716

[21]   P. Huovinen and others, Phys. Lett. B **503** (2001) 58 [arXiv:hep-ph/0101136].

[22]   D. Teaney, J. Lauret, and E.V. Shuryak, nucl-th/ 0011058.

[23] P. F. Kolb *et al.*, hep-ph/0103234

[24] T. Hirano *et al.*, these proceedings.

[25] R. S. Bhalerao, J. P. Blaizot, N. Borghini and J. Y. Ollitrault, Phys. Lett. B **627** (2005) 49

[26] F. Karsch, arXiv:hep-lat/0601013.

[27] S. S. Adler *et al.* [PHENIX Collaboration], Phys. Rev. Lett. **96** (2006) 032302

[28] M. Issah and A. Taranenko [PHENIX Collaboration], arXiv:nucl-ex/0604011.

[29] A. Adare [PHENIX Collaboration], arXiv:nucl-ex/0608033.

[30] M. Oldenburg [STAR Collaboration], arXiv:nucl-ex/0607021.

[31] M. A. C. Lamont [STAR Collaboration], arXiv:nucl-ex/0608017.

[32] M. Csanad *et al.*, arXiv:nucl-th/0512078.

[33] N. Borghini and J. Y. Ollitrault, arXiv:nucl-th/0506045.

[34] M. Csanad, T. Csorgo, R. A. Lacey and B. Lorstad, arXiv:nucl-th/0605044.

[35] S. A. Voloshin, Nucl. Phys. A **715** (2003) 379

[36] R. J. Fries, B. Muller, C. Nonaka and S. A. Bass, Phys. Rev. C **68** (2003) 044902

[37] D. Molnar and S. A. Voloshin, Phys. Rev. Lett. **91** (2003) 092301

[38] V. Greco, C. M. Ko and P. Levai, Phys. Rev. C **68** (2003) 034904

[39] K. Adcox *et al.* [PHENIX Collaboration], Phys. Rev. Lett. **89** (2002) 212301

[40] E. V. Shuryak, Nucl. Phys. A **750** (2005) 64

[41] U. W. Heinz and P. F. Kolb, Nucl. Phys. A **702** (2002) 269

[42] S. S. Adler *et al.* [PHENIX Collaboration], Phys. Rev. Lett. **94** (2005) 232302

[43] S. Okubo, Phys. Lett. **5** (1963) 165.

[44] A. Shor, Phys. Rev. Lett. **54** (1985) 1122.

[45] C. M. Ko and D. Seibert, Phys. Rev. C **49** (1994) 2198

[46] K. Haglin, Nucl. Phys. A **584** (1995) 719

[47] N. Xu, Nucl. Phys. A **751** (2005) 109.

[48] N. Borghini and J. Y. Ollitrault, Phys. Rev. C **70** (2004) 064905

[49] G. D. Moore and D. Teaney, Phys. Rev. C **71** (2005) 064904

[50] R. Rapp et al., hep-ph/0510050 (2005)

[51] S. Weinberg, Astrophys. J. , 168 (1971) 175

[52] T. Hirano and M. Gyulassy, Nucl. Phys. A **769** (2006) 71

[53] P. Kovtun, D. T. Son and A. O. Starinets, Phys. Rev. Lett. **94** (2005) 111601

[54] R. A. Lacey, arXiv:nucl-ex/0608046.

[55] R. A. Lacey *et al.*, arXiv:nucl-ex/0609025.

[56] Z. Xu and C. Greiner, Phys. Rev. C **71** (2005) 064901

[57] D. Teaney, Phys. Rev. C **68** (2003) 034913

[58] S. Gavin and M. Abdel-Aziz, arXiv:nucl-th/0606061.

[59] B. A. Gelman, E. V. Shuryak and I. Zahed, arXiv:nucl-th/0601029.

[60] A. Muronga, Phys. Rev. C **69** (2004) 044901

[61] P. Arnold, G. D. Moore and L. G. Yaffe, JHEP **0011** (2000) 001

[62] J. W. Chen and E. Nakano, arXiv:hep-ph/0604138.

[63] F. Karsch, E. Laermann and A. Peikert, Nucl. Phys. B **605** (2001) 579 [arXiv:hep-lat/0012023].

[64] C. Nonaka and M. Asakawa, Phys. Rev. C **71** (2005) 044904

[65] B. Kampfer, M. Bluhm, R. Schulze, D. Seipt and U. Heinz, Nucl. Phys. A **774** (2006) 757

[66] L. P. Csernai, J. I. Kapusta and L. D. McLerran, arXiv:nucl-th/0604032.

[67] A. Nakamura and S. Sakai, Phys. Rev. Lett. **94** (2005) 072305